DOI: https://doi.org/10.52756/ijerr.2023.v30.012 ***Int. J. Exp. Res. Rev.*, Vol. 30: 109-118 (2023)**

Original Articale | *Peer Reviewed* | *Open Access*

International Journal of Experimental Research and Review (IJERR)

ISSN: 2455-4855 (Online)
www.iaph.in

ISSN 2455-4855

Voltage stability analysis for grid-connected PV system using optimized control tested by IEEE 14 &30 bus system

Praveen Kumar Thota[1]*, Ganapathy Somaskandan[2] and Manikandan Mani[3]

[1]Department of Electrical Engineering, Annamalai University, Tamilnadu, India; [2]Department of Electrical Engineering, Annamalai University, Tamilnadu, India; [3]Department of Electrical and Electronics Engineering, Jyothishmathi Institute of Technology and Science, Karimnagar, Telangana, India

E-mail/Orcid Id:

PKT, thotap@rediffmail.com, https://orcid.org/0000-0003-2334-7325; *GS,* ganapathy1967@gmail.com, https://orcid.org/0000-0001-9547-1013; *MM,* cm.manikandan@gmail.com, https://orcid.org/0000-0002-4881-8157

Article History:

Received: 11th Jan., 2023
Accepted: 01st Apr., 2023
Published: 30th Apr., 2023

Keywords:
Grid-connected system, IEEE 14 & 30 bus, PV system, voltage stability & load demands

Abstract: In the research work presented in this paper, we present a grid-connected solar photovoltaic (PV) system, which is focused on various factors, such as the low oxide emission and high energy efficiency of the system. Solar PV systems have a greater impact on grid stability than any other energy source. IEEE 14 bus test system is used to verify the voltage stability of the bus. It is a concept of a methodology using a RNN-based PV controller in conjunction with a Landsman converter to maintain the PV system's voltage-gain ratio and improve it. Conversely, an ANN-based boost Integrated Landsman Converter improves the solar photovoltaic voltage connected to the grid. In addition, continuous monitoring of solar plants (irradiation, sunlight & voltage) is implemented through the Internet of Things (IoT). A grid voltage stability and analysis is taken by 14 buses, five generators and 12 loads test system is tested. The proposed two methods have been proven to be effective regarding the uncertainties related to loading demand. This approach offers voltage stability for grid-connected PV systems in industrial sectors. The IEEE 14 & 30 bus system tested this work using MATLAB simulation.

Introduction

The main problem of conventional power generation is CO_2 emission, which affects the environment and air. In addition, with a greater demand for coal, we need to switch from a conventional power system to a renewable one. In this renewable system, a major source is a sunlight (Solar) energy (Chowdhury, 1992). The PV source is faster than other RE sources, and there is less noise operation, among other factors. In recent years, the total cost of installing solar energy sources has decreased dramatically (Yazdani and Dash, 2009). Due to the rapid development of electrical power interfaces, the sharp drop in prices of components related to photovoltaic energy sources, and the continuation of government support programs. Solar power sources integrated into the grid are expected to increase their capacity in 2030 (Babu et al., 2021). Despite this, solar energy systems are generally recognized to be intermittent because they are dependent on solar heat and radiation (Li et al., 2020).

However, during night time, solar radiation is not available. There is no continuity of power to the grid network as a result. Changing climatic conditions, such as cloud cover, can dramatically affect the output power of a photovoltaic system, which would lead to a dramatic change in generation as a result of the change (Li et al., 2020). With intermittent energy production, the solar energy system has problems with the operation of the grid and the stability of the existing electricity grid. One of the major issues in the conventional grid inconsistent with solar energy is the voltage stability of the system. To correct the grid voltage stability, more solar energy sources are considered to estimate the grid voltage stability. Many kinds of research have been reported in the literature on the effects of grid integration of PV systems (Hou et al., 2018; Anand et al., 2018; Kumar et

***Corresponding Author:** thotap@rediffmail.com

al., 2019). For example, the study in point shows that, based on the location and depth of integration, the integration of solar panel systems can have both positive and negative effects on the stability of the electricity grid voltage (Li and Shi, 2019; Babu et al., 2019). The above research result is obtained by (Ahmad et al., 2021), who proposed an optimal solar power system and increased the grid voltage stability margin.

The electrical grid with an integrated solar energy system affects the system components in advance and creates an unstable grid voltage due to incorrect dimensions and layout. As a result, optimized technology such as a self-healing algorithm and artificial bee colony is proposed (Chandrasekar et al., 2020; Huang et al., 2019), respectively. Select the proper size and site for the solar system while considering grid stability and margin (Andrade et al., 2017). This is a simulation of the voltage fluctuation for a big T/N load demand.

The intermittency of solar electricity production, voltage fluctuations and short-term voltage deviations can increase in the low-voltage electricity distribution network, especially in fault situations (Padmanaban et al., 2019). Due to solar energy sources' increasing availability, voltage fluctuations can be negatively affected by unpredictability in electricity production (Han et al., 2018). The grid voltage stability is not properly maintained when the feeder is loaded. However, it shows that solar power source helps to maintain grid stability and provides reactive power assistance (Manikandan and Basha, 2016). When the load increases, the produced solar energy oscillates and significantly weakens the stability of the grid voltage (Moradi-Shahrbabak and Tabesh, 2018).

This research compares the IEEE 14 and 30 bus system tests of a grid-connected solar power system, the amount of solar power produced by the solar power system, and the total system load (Swain and Subudhi, 2019). The parameter was changed over time (Venkatramanan and John, 2018). A grid voltage stability index is determined by evaluating eigenvalues applied to temperature, radiation, and load parameters, which are all significant factors in grid voltage stability (Zhou et al., 2019). A comprehensive study of the effects of LSPV installation on grid voltage management can be undertaken in light of the chaotic behavior of system demand and PV generation (Kewat and Sing, 2020) and the framework provided by our study (Bana et al., 2020).

In order to provide an accurate estimate of solar power generation, the proposed method uses MATLAB simulations to account for the uncertainties associated with atmospheric changes and load requirements, including a wide range of load profiles. In addition to taking into account voltage stability margins, critical eigenvalues, and reactive and active power losses, the proposed method utilizes commonly used grid voltage stability metrics (Praveen et al., 2022). Using the IEEE 1 bus test system as an example, the proposed solution has been extensively tested using different solar power system exposure levels (Sathish et al., 2022). In addition, an IEEE 30 vector system is used to ensure the scalability of the method.

In addition to providing grid supervisors with a complete picture of the expected voltage regulation characteristics of solar PV systems, this proposal can also provide grid supervisors with a way to manage solar PV systems as they are integrated into the grid during the day. Additionally, identifying potential causes of grid instability and initiating mitigation measures can be done by using this approach.

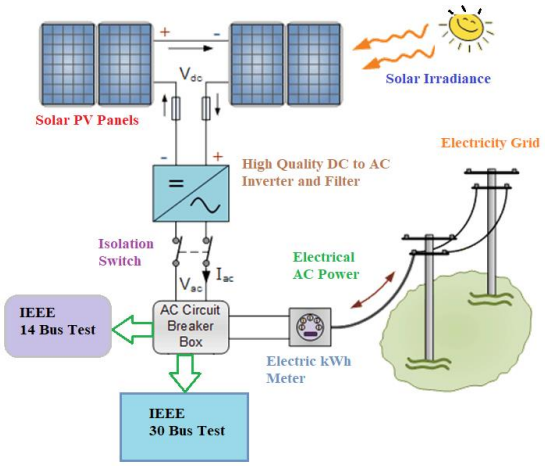

Figure 1. Solar PV system with grid connection schematic diagram

Grid-Connected PV System

During the past few years, government subsidies have played a major role in the development of grid-connected photovoltaic systems and in continuing improvements in electronic-based energy conversion systems for converting solar energy to electricity. Solar panels connect to different grid parts, from hundreds of megawatts to several kilowatts. Solar/grid-connected battery systems are described in the following sections.

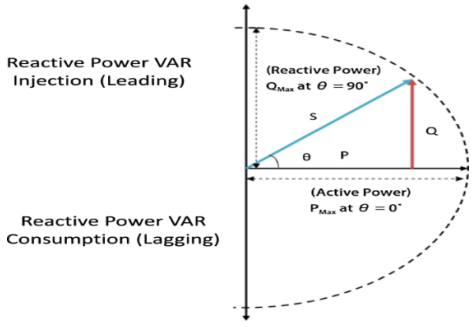

Figure 2. Graph of solar PV energy capacity.

DOI: https://doi.org/10.52756/ijerr.2023.v30.012

The Components of a PV Arrays

The main part of the solar PV system is the control unit, power electronics DC-AC inverter is the conventional PV plant depicted in figure 1. The step-up converter is used to step up the voltage of the AC grid PV generation system. The photovoltaic system combines MPPT (Maximum Power Point Tracking) control and DC-AC inverter control in the control algorithm. A large amount of electricity is generated from photovoltaic cells using MPPT control. The function of the inverter is to convert the direct current from the sun into a useful alternating current. The solar photovoltaic operating mode controls these inverters. Solar power system capacities are rated based on the connected components' volts, amperes, and output ratings.

$P^{max}_{array,dc}$ | Wmax= VMPP(Wmax) IMPP (Wmax)_____ (1)

ParrayWh = $P^{max}_{array,dc}$ |Wh_____ (2)

It is important to note that a solar cell's ability to generate reactive power is limited to between 50 and 80 watts under climatic conditions Wh(G, T) [-QavailableWh, QavailableWh], where

$$QavailableWh = \sqrt{S_{PV}^{max^2} - PPV} \,|W2 \_\_\_\_\_ (3)$$

This figure shows the capacity curve of the solar system, with the semicircle representing the range of operation (Fig. 2). PP V represents the PV system's output power, while Qmax and Qmin represent its phantom power capability. The diameter of the semicircle reflects its MVA rating and the radius of the system's MVA rating.

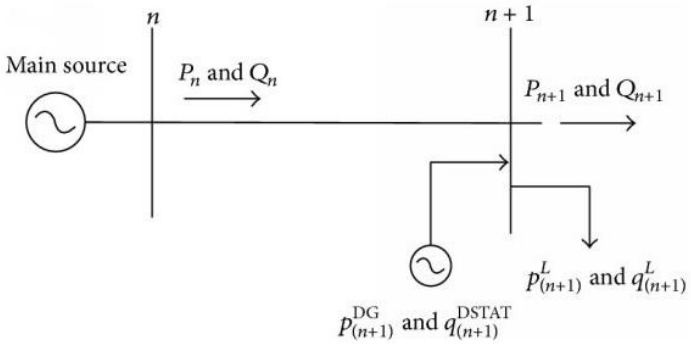

Figure 3. A simplified two-bus architecture

In order to maintain grid voltage stability, PV systems with high penetration play an important role by providing phantom current capacity to the grid. It is crucial to remember that solar systems can only support reactive power if the associated grid can also support it. Depending on the GC's requirements, a solar system's reactive or phantom power can be changed in the pf mode or voltage mode to meet the GC's requirements.

Grid voltage Regulation Analysis

An electrical system with good regulation of voltage can maintain a uniform voltage at each bus without any external disturbances and under normal conditions under normal conditions as well (Babuet al., 2021). In case of faulty electrical systems, overloaded machines, or insufficient reactive power present in the system, anunstable voltage may result. In order to understand the effect of the unstable nature of solar power generation on a carrier voltage integrated into a compact dual-carrier system, take a look at figure 3.

In this system, a load vector is depicted as 'i' (voltage shown as Vi) and a solar source has been integrated into the power vector 'j' (voltage Vj) through the line Z=1,Y =G+jB=Y ∠θ. Considering the double bus system that is considered, the energy transfer from bus 'i' to bus 'j' is as follows:

SL–Sarray=(|Vj|*|Vi|∠(δi−δj)−|Vj||Vi|)* |Y|∠−θ_____ (4)

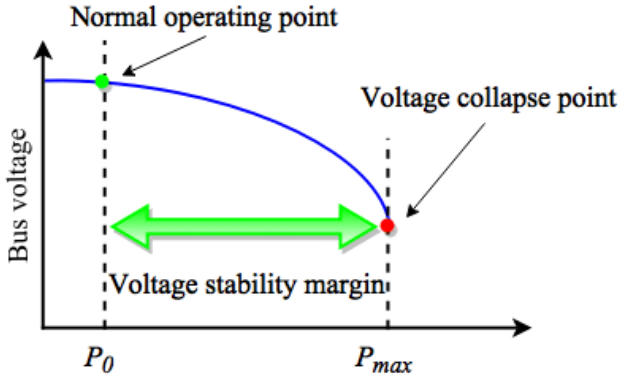

Figure 4. The voltage on the load bus will vary in a two-bus system with a variable PV system capacity

Consider now that the PV S array is the power generation array formed by the array P + jQ and the load demand array is formed by the array PL + jQL. In this matrix P, the energy that the solar system produces at time t is the energy that it extracts from the atmosphere at that time, which in this case is the solar energy at time t under given atmospheric conditions Wt = (Gt, Tt) are taken. Based on equation (4) for the real and imaginary power transfer from bus 'i' to bus j, the reactive output power of the photovoltaic system can be calculated as follows:

Step: 1 The real power is taken and transfer from bus "i" to "j"

Step: 2 The reactive power is consider and transfer from bus "i" to "j"

Step: 3 Real transfer "i" to "j" connected in PV array minus load demand in real power.

DOI: https://doi.org/10.52756/ijerr.2023.v30.012

Step: 4 Reactive power "i" to "j" connected in PV array minus load demand in reactive power

Step: 5 the load angle is taken $\gamma = \delta i - \delta j - \theta$.

Step: 6 by adding the steps 3,4 and take squaring both side we get $P_{ij}^2 (1 + \beta 2)$ (5)

Equation (5) is illustrated in Section 3 in Figure 4 and the load bus voltage changes are shown to illustrate the effects of changing the output outputting solar power on the bus voltage, specifically for a variable potential PV system (called PV PV) and a lagging load of 10.0 MW with 0.960 pf, respectively. According to the weather conditions, the amount of solar power a bus can generate and its reactive power reserve can vary (Parray). The bus voltage can take into account constant load requirements even when there is a constant load requirement. Considering both the uncertainty of load demand, as well as the power generated by the PV system, it is important to understand the impact that solar energy penetration will have on grid voltage regulation. A Monte Carlo simulation framework is presented below that uses the Monte Carlo simulation technique to examine the effect of PV integration on grid voltage stability.

Methodology

The PV system's grid voltage stability is maintained, increased solar energy from the PV array is to be analysed and a framework based on Monte-Carlo iteration is implemented. Due to climatic changes and load demands, PV electricity production is unpredictable. Moreover, a proposed method to determine grid stability is reactive power for hourly predicted and line losses. These values are analysed by following steps:

Step 1: For each bus in the power grid, data is collected for the load demand and PV system power generation and processed in a structured manner to facilitate grid efficiency.

Step 2: The data set should then be statistically analysed in order to generate a probability distribution of load demand and PV system power generation for each hour in a day using the data set

Step 3: Input variables for Montic Carlo simulation: For each of the load buses and PV systems in the power grid, here is the probability distribution of the load demand and PV system power generation in its hour in relation to the power grid as a whole.

Step 4: Montic carlo Iteration (Ns) is taken from step 3.

Step 5: By taking random samples from the corresponding probability distribution each hour in the i^{th} hour, generate demand and power generation samples for each of the load buses and PV systems in the power grid in order to generation demand and power generation samples.

Step 6: An analysis of the model, a QV analysis, and an analysis of the load flow should be performed.

Step 7: Indicators of voltage stability, eigenvalues, QV margins, and line losses are calculated.

Step 8: If Ns iterations completed, Calculate the expected value of each indicator. If Ns iterations not completed do the step 4.

Step 9: To stop the process if Ns is completed.

Evaluation of voltage stability

As a first step, it would be interesting to collect the actual electricity demand of the load bus along with the solar power production data produced in the grid's PV cells. In the second step of the process, an uncertainty load demand profile is collected and a lack of PV generation is presented. Statistical analysis of the samples is conducted on an hourly basis. Equation 6 can be used to calculate and predetermine this.

$$\mathbb{P}_{L,i}^{hr,k} \sim \mathcal{N}\left(\mu_{L,i}^{hr,k}, \sigma_{L,i}^{hr,k^2}\right) \text{ and } \mathbb{P}_{PV,i}^{hr,k} \sim \mathcal{N}\left(\mu_{PV,i}^{hr,k}, \sigma_{PV,i}^{hr,k^2}\right) \_(6)$$

In equation 8. with cells representing probability density functions and ND with mean and standard deviation, Simile definition is applicable to $\mathbb{P}_{PV,i}^{hr,k}$.

Monte Carlo Iteration

In the model analysis of power flow assessment and reactive power voltage of the system, Ns time for every hour of the day is taken into the process. Lastly, a randomised sample of input samples is given below for each of these methods.

A specific probability density distribution, and power factor in maximum and minimum values are selected based on the load power factor in the i^{th} bus, and a uniform distribution is also considered. It is determined that the solar power action of each energy source at the k^{th} hour is determined by selecting a random sample from their probability distribution.

$$P_{array,i}^{Hr,k} = \mathbb{R}\left[\mathbb{P}_{array,i}^{Hr,k} \sim \mathcal{N}\left(\mu_{array,i}^{Hr,k}, \sigma_{array,i}^{Hr,k^2}\right)\right] \_\_\_\_\_ (7)$$

i^{th}bus only has a limited amount of reactive power $\left[-Q_{array,i}^{Hr,k}, Q_{array,i}^{Hr,k}\right]$, 24-hour with an MVA rating$S_{array,i}^{max}$.

$$Q_{array,i}^{Hr,k} = \left[S_{array,i}^{max^2} - P_{array,i}^{Hr,k^2}\right]\text{^}1/2 \_\_\_\_\_ (8)$$

A voltage regulation indicator produces the integration results for Ns time of 24 hours.

Result and Discussion

Consider using the IEEE 1 bus system for testing. IEEE 1-bar systems consist of 11 constant current loads, 1 bar, and 20 branches, each of which consists of three (3) synchronous compensators and five (5) synchronous

DOI: https://doi.org/10.52756/ijerr.2023.v30.012

generators. As shown in figure 5, evaluate the platform voltage level and obtain the factors that influence the load bus.

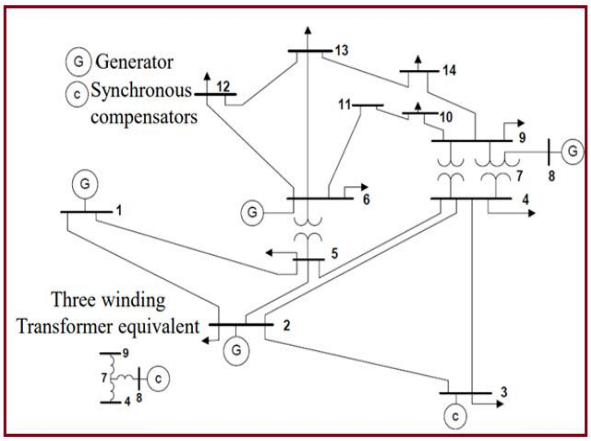

Figure 5. Standard IEEE 14 bus system (Padmanaban et al., 2019)

By using the reactive voltage curve method, it is possible to calculate the reactive power margin for a load carrier by examining the values of the reactive voltage curve part of the load carrier. There are two graphs shown in Figure 7 and Figure 8 that show how the QV curve and rod cofactors are analysed in the base case, respectively. As you can see from the above table, the reactive power margins of buses 103.28, 110.78, 5.13 and 539.10 are respectively 103.28, 158.78, 5.13 and 539.10 MW. Two buses have the most participation: bus number 1 and bus number 10 (0.33 and 0.23, respectively). There is a 0.00890 duty factor on bus 4 and a 0.00390 duty factor on bus 5. Bus 1 and Bus 10 are the weakest of all buses. Buses4, 5 are strong nodes on other buses.

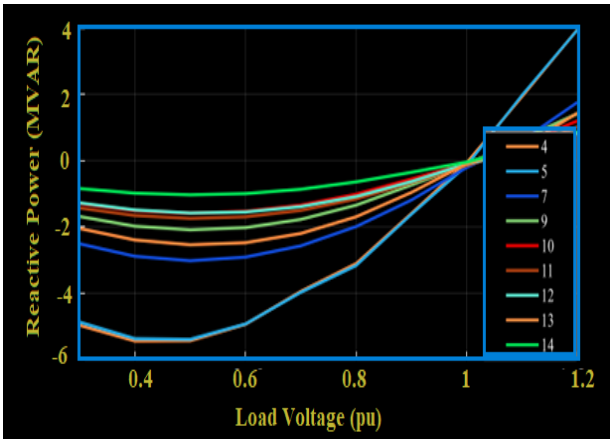

Figure 6. The reactive power curves of the IEEE 14 bus system and the voltage curves of the load buses

It is shown in figure 6 that the reactive power and load voltage graphs, in which the 14 buses are shown to carry all the load demands and the voltage profile for each bus. As a result, it can be clearly seen that a 12-bus system is weak in load and voltage stability.

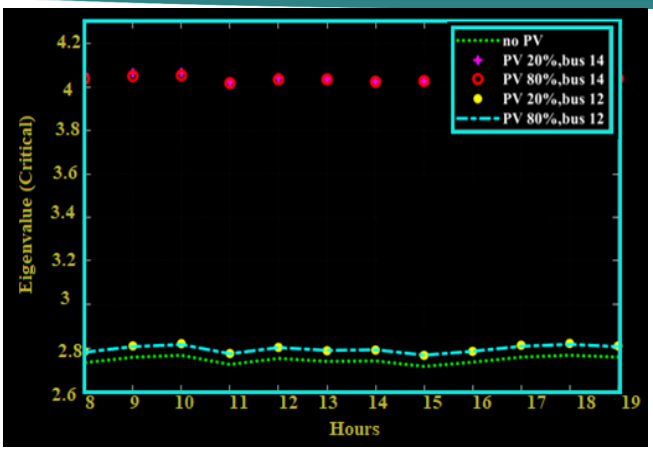

Figure 7. Rates of photovoltaic installation on various types of buses

A comparison of the rates of PV installations for weak buses is shown in figure 7. It is evident in this graph that 14 buses are weakened, and 80% of PV are connected according to the time and also, the 12th bus is weakened, and 20% of PV are connected according to the time

Instance I: Bus system of IEEE 14

The grid-connected PV system is considered for IEEE 14 bus approach. It takes strong and poor nodes to analyse voltage stability even the load demand is increased. In the test system at weaker bus PV system is implemented. In an IEEE 14 bus structure,4 loads are unexpected profiles produced from 11 loads using standard deviations of hourly samples taken from 4 industrial loads. As per the analysis of industrial and domestic loads 3 business load profiles and four residential load profiles are produced. To evaluate the factious load requirement, power factors are assumed to vary 0.85 to 0.95. PV ratings are normally determined with a full load of the solar module which is linked in a weaker bus. An hourly mean and SD data are evaluated with ratings of 80.9%, 52% and 20% of linked bus total loads 12.1 MW, 8.50 MW and 3.9 MW respectively in this study. In one of the proposed approaches (which models a PV controller using RNNs based on a Landsman transformer), the expected value of each of the metrics based on the characteristics of the load is calculated using Monte Carlo simulations based on the HM and SD of the load as input data for the Monte Carlo iterations. There are two slots available in PV integration, which are 12 buses and 1 bus. We optimised the test system based on the critical eigenvalues, as shown in figure 8. During each solar hour of the day (8:00 a.m. to 7:00 p.m.), it is considered that buses 10 and 1, without solar panels on their roofs, are solar-powered penetrance in 19.9% and 81%.

DOI: https://doi.org/10.52756/ijerr.2023.v30.012

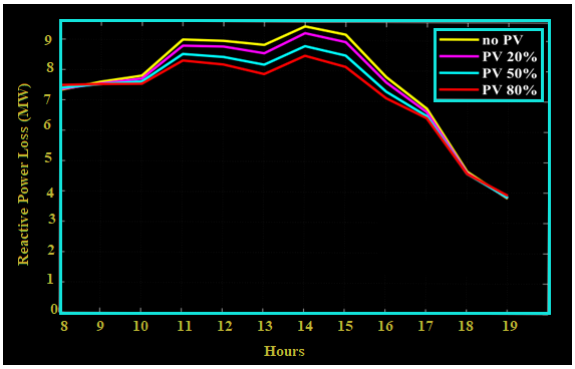

Figure 8. The amount of true power loss for various levels of PV exposure is expressed in megawatts (MW)

Compared to bus 12, the PV location at bus 1 increases the critical eigen value compared to bus 12. A total active power loss and a total reactive power loss are shown in Figures 9 and 10 for different levels of solar power of 20.0%, 50.0%, and 80.0%.The maximum hours of solar radiation are from 10:00 a.m. to 03:00 a.m. The expected peak power for the solar cycle is shown in figure 11. An interaction analysis of voltage and potential was performed using the structure and Monte Carlo iterations. The combination of PVPP shows a higher reactive power margin than a system without PV.

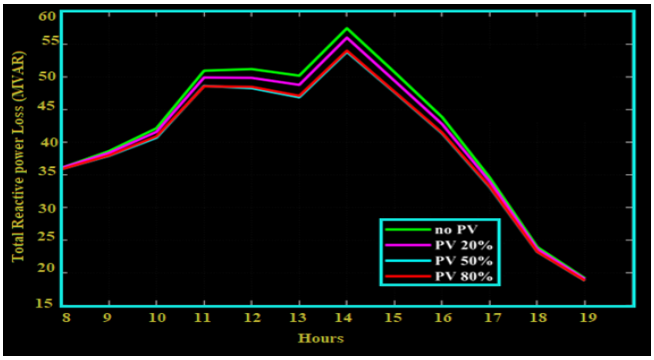

Figure 9. Different reactive power loss (MVAR) for hourly in a day

As shown in figure 9, the total reactive power losses may be calculated according to the time of day. It is required to penetrate PV percentage to compensate losses. For instance, 80% of PVs are connected to the weak bus and 20% are connected to the storage bus. There is a possibility that the voltage stability and the reactive power losses may increase in this situation.

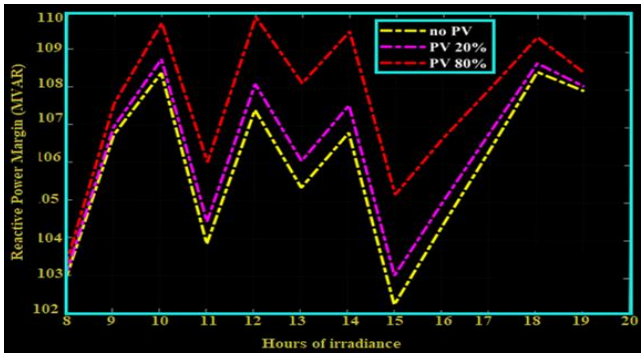

Figure 10. RPM (MVAR) at various penetration levels

Furthermore, the PV penetration results showed an 80% increase in reactive power at 0.8 meV. The probability distributions of critical eigenvalues of marginal reactive power at different time periods from 9:00 to 12:00 and 18:00 are shown in figures 11 and 12, respectively.

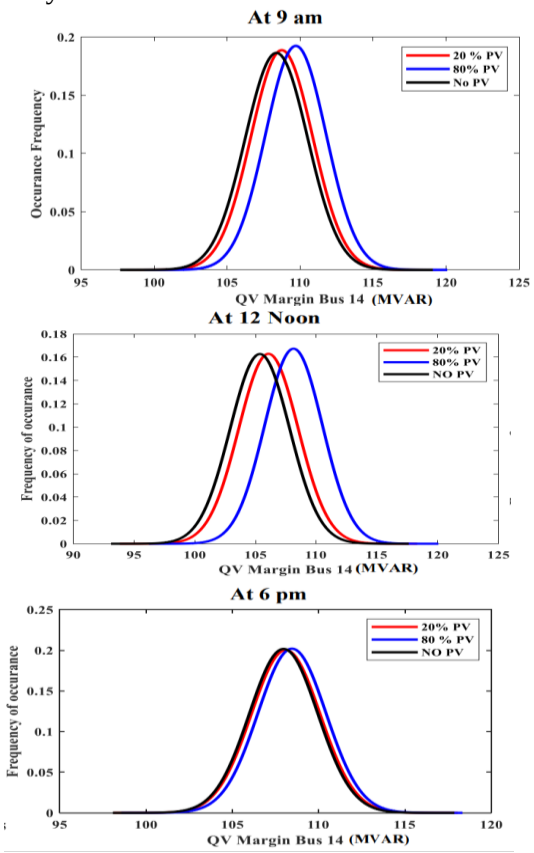

Figure 11. Variations in PV penetration at bus 14 with the reactive power margin

This figure illustrates the reactive power margin which is available at bus 14 at different times with varying levels of PV penetration. There is no doubt that the reactive power margin at the time of 9 am indicates a very high level of reactivity. There is a decrease in the reactive power margin at 12 noon and an increase in the reactive power margin at 6 pm compared with 12 noon.

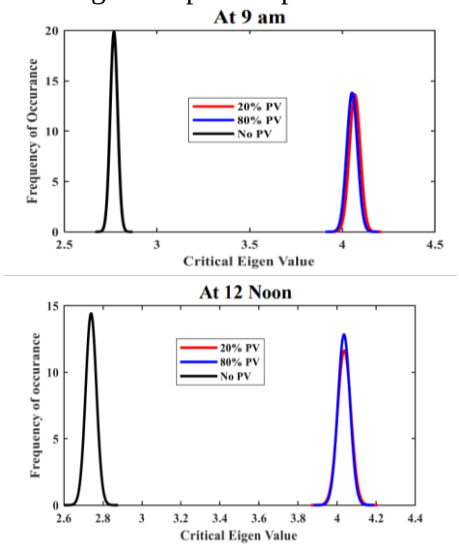

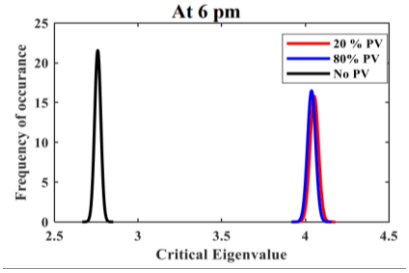

Figure 12. 14 bus PV penetration with normal eigenvalue distribution

According to figure 13, When compared to other PV penetrations and non-photovoltaic penetrations, PV penetration has the highest probability of increasing this margin.

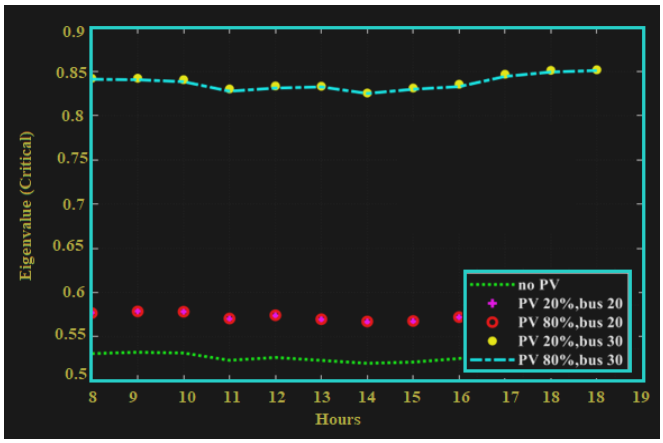

Figure 14. Various solar penetrating rates of Critical Eigenvalue

Instance II: IEEE 30 bus system

The IEEE 30 bus system considers the multiple charging requirements of PV systems and suggests methods for solar grid-connected systems. Considering the weakest node in this system, the individual PV penetrations are 20%, 50%, and 80%, respectively. Solar radiation was discovered after extensive research. The figures 14 and 15 present the results as critical eigenvalues, total real power loss, and the reactive power margin Q for an IEEE 30-bus system during a solar day for the two figures 14 and 15.

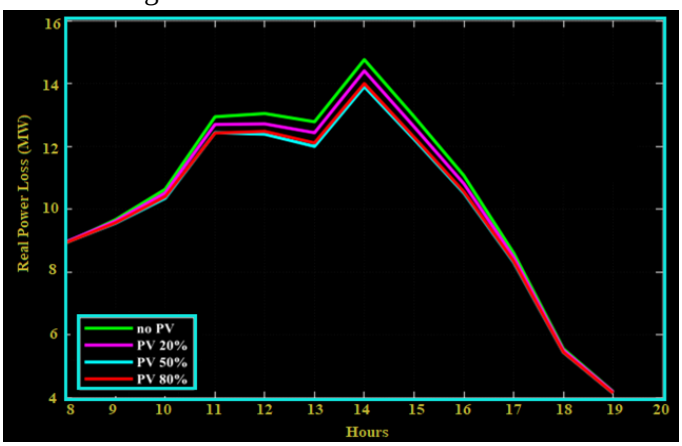

Figure 15. The overall true power loss (MW) for various degrees of PV penetration

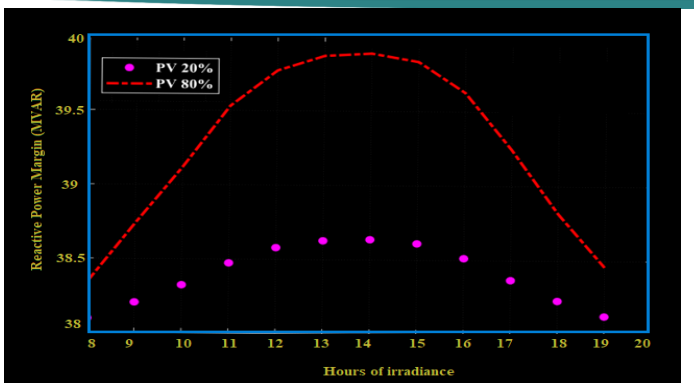

Figure 13. Reactive power margin (MVAR) for various solar perforation levels'

Solar energy is the most powerful system in the field of renewable energy. In this case, the dependent power supply of the inverter is isolated from the grid. Any power-based synchronous generator inertial support is not frequency compatible. The result is a shift in the highest frequency (RoCoF), and the network can be more sensitive to network interference.

Effect on Harmonics

As harmonics increase the load demand on the distribution system, the result is an increase in active power losses in transformers, transmission lines, generators, and load resistors, which in turn leads to a decrease in the thermal efficiency of the distribution system. The results of studies (Babu et al., 2021) compared sinusoidal (systems with only linear loads) to non-sinusoidal (systems with both linear and non-linear loads) conditions have concluded that harmonics have a negative effect on voltage stability (systems with both linear and non-linear loads). Moreover, as the current of the nonlinear load increases (Sanepalleet al., 2022), the maximum power transmission decreases, and the bus bar with the highest nonlinear load in the system is one of the most affected bus bars in the entire system. A non-linear load causing harmonics to be generated in the transmission system can generally limit its transmission capacity and voltage stability due to the presence of harmonics caused by non-linear load characteristics. The further problem is that harmonics generated by PV transducers can compromise grid reliability and reduce equipment performance in other areas (Abdul, 2020). The on-going harmonisation process can lead to overheating or malfunctioning equipment, tripping protective relays (Moyo et al., 2021), and damaging critical loads like hospital equipment.

In addition, harmonics can cause the transformer and coil to become saturated, leading to increased core losses as a result. Before injecting the PV output into the grid, the total harmonic distortion (THD) value should

DOI: https://doi.org/10.52756/ijerr.2023.v30.012

be checked to see if it is within the allowable range of the relevant grid code (Grossi and Buscema, 2007). If the THD value exceeds the allowed range of the grid-connected code, the corresponding PV system will be placed in the form of islands (Azadani et al., 2012).

PWM inverters can manage THD values and harmonics with the correct PWM method. It is possible to reduce the amount of harmonics injected into the grid by adding active filters to PV converters (Tielens and Hertem, 2016). PV converters can also be configured to suppress harmonics caused by non-linear loads using advanced technologies such as load current harmonic compensators. Policies can be established to provide financial incentives to inverter owners to eliminate these harmonics. Using a suitable PWM strategy, the PV inverter can control the THD value and subsequent harmonics. Adding active filters to PV converters can reduce the amount of harmonics injected into the grid (Milano et al., 2018). Furthermore, PV converters can suppress harmonic distortion caused by nonlinear loads by using advanced technologies such as load current harmonic compensators.

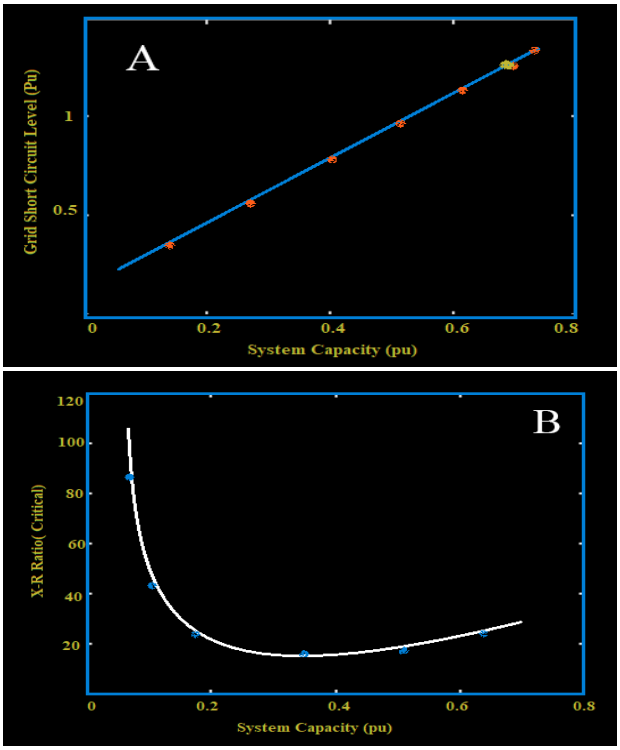

Figure 16. (a) Grid short circuit level and (b) Grid X-R ratio for incorporating a Pmax-capable solar farm

In figure 16(a) and (b), we can see the level of grid short-circuit and the ratio of grid X-R for grid-connected PV systems installed in solar farms compliant with Pmax regulations. The figure below shows the minimum grid short-circuits level and the X-R ratio, which refers to the grid's X-R ratio compared to the PV system's capacity. (a) Assume network resistance Rg = 0.050pu @ 100.0 MVA and 132.0 kV.

First, the grid-connected PV system uses an optimized RNN-based controller to compensate for the voltage fluctuation when the converter output is connected to grid with IEEE14& 30 bus system. A PV array is connected in weak buses for testing in both test systems.

Secondly, the grid-connected PV system uses an optimized ANN-based controller is connected. The grid voltage was maintained as stable while the load bus was connected to the PV grid. The converter, grid, and load bus voltages were the same for reactive power deviation.

Finally, the solar irradiation, temperature, or short-circuit conditions are measured by the IOT platform. The IOT senses the fault and error signal to the cloud. It controls power generation and maintains a constant generation of power to satisfy grid stability.

Conclusion

This work mainly emphasised analysing a grid-connected PV power system with voltage stability on IEEE 14 bus & 30 bus system. In this analysis, there are two approaches taken. RNN-based PV controllers and ANN-based PV controllers are tested by IEEE 14 and 30 bus system. The DC-DC converter for both methods is Landsman Converter. Generally, a load demand bus is connected to the PV module, and the voltage stability is maintained even in the distribution side load demand. The weak buses are not getting stability because solar irradiance is not constant. In addition, the research shows that a static synchronous compensator is present to achieve reactive power compensation at weak buses at 14 and 30 systems. The proposed RNN & ANN controller assesses the value of the voltage stability performance purely based on solar irradiance, which is analysis time from 9 am to 6 pm.

For IEEE 14, bus methods are used to calculate the stability by Monte Carlo simulation, and for IEEE30, bus system methods are used to calculate the voltage stability by critical eigenvalue analysis. These two methods observe with two test systems. As a result of the comparison, the average consumption of a load of an array is connected to a weak bus, increasing PV performance and decreasing the line losses. In addition, the reactive power margin is boosted for the load bus from 10 am to 3 pm.

Acknowledgement

Annamalai University & Jyothishmathi Institute of Technology and Science provided the laboratory facilities and support for this study, which the authors gratefully acknowledge. The Departments of Higher Education,

Science and Technology, are all acknowledged by the authors. Annamalai University's support in carrying out this research work.

Conflict of Interest

None

References

Abdul, R.A. (2020). Solar PV System for Water Pumping Incorporating an MPPT based Bat Optimization Circuits and Systems. *Journal of Advanced Research in Dynamical and Control Systems*, *12*(01-Spl. Issue), 786-794. https://doi.org/10.5373/JARDCS/V12SP1/20201130

Ahmad, M.W., Gorla, N.B.Y., Malik, H., & Panda, S.K. (2021). A Fault Diagnosis and Post fault Reconfiguration Scheme for Interleaved Boost Converter in PV-Based System. *IEEE Transactions on Power Electronics*,*36*(4), 3769-3780. https://doi.org/10.1109/TPEL.2020.3018540

Anand, I., Senthilkumar, S., Biswas, D., & Kaliamoorthy, M. (2018). Dynamic Power Management System Employing a Single-Stage Power Converter for Standalone Solar PV Applications. *IEEE Transactions on Power Electronics*, *33*(12), 10352-10362. 10.1109/TPEL.2018.2804658

Andrade, A.M.S.S., Schuch, L., da Silva, M.M.L. (2017). High Step-Up PV Module Integrated Converter for PV Energy Harvest in FREEDM Systems. *IEEE Transactions on Industry Applications*, *53*(2), 1138-1148. 10.1109/TIA.2016.2621110

Azadani, E.N., Cañizares, C.A., & Bhattacharya, K. (2012). Modeling and stability analysis of distributed generation. 2012 IEEE Power and Energy Society General Meeting, IEEE, pp. 1-8. https://doi.org/10.1109/PESGM.2012.6345141

Babu, V., Ahmed, K.S., Shuaib, Y.M., & Manikandan, M. (2021). Power Quality Enhancement Using Dynamic Voltage Restorer (DVR)- Based Predictive Space Vector Transformation (PSVT) With Proportional Resonant (PR)-Controller. *IEEE Access*, *9*, 155380-155392. https://doi.org/10.1109/ACCESS.2021.3129096

Babu, V., Basha, S.S., Shuaib, Y.M., Manikandan, M., & Enayathalis, S. (2019). A novel integration of solar fed dynamic voltage restorer for compensating sag and swell voltage in distribution system using enhanced space vector pulse width modulation (ESVPWM). *Universal Journal of Electrical and Electronic Engineering*, *6*(5), 329-350. 10.13189/ujeee.2019.060504

Bana, P.R., Panda, K.P., Padmanaban, S., Mihet-Popa, L., Panda, G., & Wu, J. (2020). Closed-Loop Control and Performance Evaluation of Reduced Part Count Multilevel Inverter Interfacing Grid-Connected PV System. *IEEE Access*, *8*, 75691-75701. 10.1109/ACCESS.2020.2987620

Chandrasekar, B., Nallaperumal, C., Padmanaban, S., Bhaskar, M.S., Holm-Nielsen, J.B., Leonowicz, Z., & Masebinu, S.O. (2020). Non- Isolated High-Gain Triple Port DC–DC Buck-Boost Converter With Positive Output Voltage for Photovoltaic Applications. *IEEE Access*, *8*, 113649-113666. https://doi.org/10.1109/ACCESS.2020.3003192

Chowdhury, B.H. (1992). Optimizing the integration of photovoltaic systems with electric utilities.*IEEE Transactions on Energy Conversion*, *7*(1), 72-78. https://doi.org/10.1109/60.124544

Grossi, E., & Buscema, M. (2007). Introduction to artificial neural networks. *European Journal of Gastroenterology & Hepatology*, 19(12), 1046-1054. 10.1097/MEG.0b013e3282f198a0

Han, B., Lai, J.S., & Kim, M. (2018). Dynamic Modeling and Controller Design of Dual-Mode Cuk Inverter in Grid- Connected PV/TE Applications. *IEEE Transactions on Power Electronics*,*33*(10), 8887-8904. 10.1109/TPEL.2017.2779843

Hou, X., Sun, Y., Han, H., Liu, Z., Su, M., Wang, B., & Zhang, X. (2018). A General Decentralized Control Scheme for Medium-/High-Voltage Cascaded STATCOM.*IEEE Transactions on Power Systems*, *33*(6), 7296-7300. https://doi.org/10.1109/TPWRS.2018.2865127

Huang, Q., Huang, A.Q., Yu, R., Liu, P., & Yu, W. (2019). High-Efficiency and High-Density Single-Phase Dual-Mode Cascaded Buck–Boost Multilevel Transformer less PV Inverter With GaN AC Switches. *IEEE Transactions on Power Electronics*,*34*(8), 7474-7488. https://doi.org/10.1109/TPEL.2018.2878586

Kewat, S., & Singh, B. (2020). Grid Synchronization of WEC-PV-BES Based Distributed Generation System Using Robust Control Strategy. *IEEE Transactions on Industry Applications*, *56*(6), 7088-7098. 10.1109/TIA.2020.3021060

Kumar, N., Singh, B., Panigrahi, B.K., & Xu, L. (2019). Leaky-Least- Logarithmic-Absolute-Difference-Based Control Algorithm and Learning-Based InC MPPT Technique for Grid-Integrated PV System. *IEEE Transactions on Industrial Electronics*, *66*(11), 9003-9012. https://doi.org/10.1109/TIE.2018.2890497

Li, C., Burgos, R., Wen, B., Tang, Y., & Boroyevich, D. (2020). Stability Analysis of Power Systems With Multiple STATCOMs in Close Proximity. *IEEE Transactions on Power Electronics*, *35*(3), 2268-2283. 10.1109/TPEL.2019.2931891

Li, R., & Shi, F. (2019). Control and Optimization of Residential Photovoltaic Power Generation System With High Efficiency Isolated Bidirectional DC–DC Converter. *IEEE Access*, *7*, 116107-116122. 10.1109/ACCESS.2019.2935344

Manikandan, M., & Basha, A.M. (2016). ODFF: Optimized Dual Fuzzy Flow Controller Based Voltage Sag Compensation for SMES-Based DVR in Power Quality Applications. *Circuits and Systems*, *7*(10), 2959-2974. https://doi.org/10.4236/cs.2016.710254

Milano, F., Dorfler, F., Hug, G., Hill, D.J., & Verbi, G. (2018). Foundations and challenges of low-inertia systems. *Power Systems Computation Conference* (PSCC), IEEE, pp. 1–25. https://doi.org/10.23919/PSCC.2018.8450880

Moradi-Shahrbabak, Z., & Tabesh, A. (2018).Effects of Front-End Converter and DC-Link of a Utility-Scale PV Energy System on Dynamic Stability of a Power System. *IEEE Transactions on Industrial Electronics*, *65*(1), 403-411. https://doi.org/10.1109/TIE.2017.2721902

Moyo, R.T., Tabakov, P.Y., & Moyo S. (2021). Design and Modeling of the ANFIS-Based MPPT Controller for a Solar Photovoltaic System. *Journal of Solar Energy Engineering*, *143*(4), 041002. https://doi.org/10.1115/1.4048882

Padmanaban, S., Priyadarshi, N., Bhaskar, M.S., Holm-Nielsen, J.B., Hossain, E., & Azam, F. (2019). A Hybrid Photovoltaic-Fuel Cell for Grid Integration With Jaya-Based Maximum Power Point Tracking: Experimental Performance Evaluation. *IEEE Access*, *7*, 82978-82990. https://doi.org/10.1109/ACCESS.2019.2924264

Praveen, K.T., Ganapathy, S., & Manikandan, M. (2022). Improvement of voltage stability for grid connected solar photovoltaic systems using static synchronous compensator with recurrent neural network. *Electrical Engineering & Electromechanics*, *2*, 69-77. https://doi.org/10.20998/2074-272X.2022.2.10

Sanepalle, G.R., Ganapathy, S., & Manikandan, M. (2022). Three Phase Four Switch Inverter Based DVR for Power Quality Improvement With Optimized CSA Approach. *IEEE Access*, *10*, 72263-72278. 10.1109/ACCESS.2022.3188629

Sathish, Ch. Chidambram, I.A., & Manikandan, M. (2022) Reactive Power Compensation in a Hybrid Renewable Energy System through Fuzzy Based Boost Converter. *Problemele Energeticii Regionale*, *53*(1), 10-26. https://doi.org/10.52254/1857-0070.2022.1-53.02

Swain, S., & Subudhi, B. (2019). Grid Synchronization of a PV System With Power Quality Disturbances Using Unscented Kalman Filtering. *IEEE Transactions on Sustainable Energy*, *10*(3), 1240-1247. 10.1109/TSTE.2018.2864822

Tielens, P., & Hertem, D.V. (2016). The relevance of inertia in power systems. *Renewable and Sustainable Energy Reviews*, 55, 999–1009. https://doi.org/10.1016/j.rser.2015.11.016

Venkatramanan, D., & John, V. (2018). Dynamic Modeling and Analysis of Buck Converter based Solar PV Charge Controller for Improved MPPT Performance. *IEEE International Conference on Power Electronics, Drives and Energy Systems (PEDES)*, pp. 1-6. 10.1109/TIA.2019.2937856

Yazdani, A., & Dash, P.P. (2009). A Control Methodology and Characterization of Dynamics for a Photovoltaic (PV) System Interfaced With a Distribution Network. *IEEE Transactions on Power Delivery*, *24*(3), 1538-1551. https://doi.org/10.1109/TPWRD.2009.2016632

Zhou, Y., Ho, C.N.M., & Siu, K.K.M. A. (2019). Fast PV MPPT Scheme Using Boundary Control With Second-Order Switching Surface. *IEEE Journal of Photovoltaics*, *9*(3), 849-857. https://doi.org/10.1109/JPHOTOV.2019.2899470

How to cite this Article:

Praveen Kumar Thota, Ganapathy Somaskandan and Manikandan Mani (2023). Voltage stability analysis for grid-connected PV system using optimized control tested by IEEE 14 &30 bus system. *International Journal of Experimental Research and Review*, *30*, 109-118.

DOI : https://doi.org/10.52756/ijerr.2023.v30.012